Tropospheric Oxidation Mechanism of Dimethyl Ether and Methyl Formate

David A. Good and Joseph S. Francisco*

Department of Chemistry and Department of Earth and Atmospheric Sciences, Purdue University, West Lafayette, Indiana 47907-1393

Received: June 16, 1999; In Final Form: November 9, 1999

The oxidation mechanism of dimethyl ether is investigated using ab initio methods. The structure and energetics of reactants, products, and transition structures are determined for all pathways involved in the oxidation mechanism. The detailed pathways leading to the experimentally observed products of dimethyl ether oxidation are presented. The energetics of over 50 species and transition structures involved in the oxidation process are calculated with G2 and G2(MP2) energies. The principal pathway following the initial attack of dimethyl ether (CH_3OCH_3) by the OH radical is the formation of the methoxymethyl radical (CH_2OCH_3). Oxidation steps lead to the formation of methyl formate, which is consistent with the experimentally observed products. Oxidation pathways of methyl formate are also considered.

I. Introduction

Concerns about mobile source emissions and their impact on urban tropospheric ozone formation have spurred research into the development of alternative fuels. Engine makers and automotive companies are looking for ways to decrease emissions of CO and NO_x. Fuel composition affects the tendency of a fuel to form soot particles and NO_x. Increasing the carbon-to-hydrogen ratio or the number of carbon−carbon bonds increases the tendency of a fuel to form soot. Oxygenated hydrocarbons, such as ethers, can be added to fuels to maintain performance while lowering tailpipe emissions of CO. Dimethyl ether (DME) is a fuel antiknock agent and proposed diesel fuel substitute. DME has been used as a methanol ignition improver in diesel engines, where it has been reported to reduce hydrocarbon emissions. Some of its attractive features include low self-ignition temperature, low octane number (high cetane number, 55−60), reduced combustion noise, particle emission and NO_x emissions. DME-fueled engines are nonsooting, and DME can economically be produced from a one-step synthesis. Engine tests have shown that DME-fueled diesel engines have emission levels that surpass the California Ultralow Emissions Vehicle (ULEV) regulation for medium duty vehicles.[1] Many investigators have studied the fate of dimethyl ether in combustion applications. Studies by Askey et al.[2] and Urey et al.[3] determined that the thermal decomposition of dimethyl ether followed first-order kinetics. Benson later proposed that CO bond fission (eq 1a) initiated a chain of thermal degradation

$$CH_3OCH_3 \rightarrow CH_3 + CH_3O \qquad (1a)$$

reactions.[4,5] The barrier for this reaction was estimated at 81.1 kcal mol^{-1}. Product studies found concentrations of CH_2O, C_2H_6, H_2, and CH_4. The formation of C_2H_6, CH_2O, and CH_4 was explained by the following mechanism.

$$CH_3 + CH_3 \rightarrow C_2H_6 \qquad (1b)$$

$$CH_3 + CH_3OCH_3 \rightarrow CH_4 + CH_2OCH_3 \qquad (1c)$$

$$CH_2OCH_3 + (M) \rightarrow CH_3 + CH_2O + (M) \qquad (1d)$$

The net result of eqs 1c and 1d is the conversion of dimethyl ether into CH_4 and CH_2O via CO bond cleavage. Evidence was presented by Pottie et al.[6] suggesting that CH bond cleavage could compete with CO bond cleavage in mercury, photosensitized decomposition experiments, i.e., reaction 2. Nash et al.[7]

$$CH_3OCH_3 \rightarrow CH_2OCH_3 + H \qquad (2)$$

identified 1,1 elimination of H_2 (eq 3) and 1,2 elimination of CH_4 (eq 4) as competitive channels using ab initio methodology.

$$CH_3OCH_3 \rightarrow CH_3OCH + H_2 \qquad (3)$$

$$CH_3OCH_3 \rightarrow CH_4 + CH_2O \qquad (4)$$

Thus, the formation of CH_4 and CH_2O can be explained by reactions 1c and 1d via CO bond cleavage or by reaction 4, which proceeds through a four-centered transition structure. Reaction 3 is a possible explanation for the detection of hydrogen in previous experimental investigations. Reactions 1c and 2 yield the CH_2OCH_3 radical as a product, yet only one reaction (1d) describes its fate. A thorough investigation into the possible thermal degradation channels of CH_2OCH_3 has yet to be undertaken.

The atmospheric oxidation of DME has been studied by Japar et al.,[8] Jenkin et al.,[9] Wallington et al.,[10] Langer et al.,[11] and Sehested et al.[12,13] The first step involves abstraction of a hydrogen atom from dimethyl ether by the tropospheric hydroxyl radical, eq 5. The CH_3OCH_2 radical may participate in one of

$$CH_3OCH_3 + OH \rightarrow CH_2OCH_3 + H_2O \qquad (5)$$

three channels, as proposed by Sehested et al.[13]

$$CH_2OCH_3 + M \rightarrow CH_3 + CH_2O + M \qquad (1d)$$

$$CH_2OCH_3 + CH_2OCH_3 \rightarrow \text{products} \qquad (6a)$$

$$CH_2OCH_3 + O_2 + M \rightarrow O_2CH_2OCH_3 + M \qquad (6b)$$

$$CH_2OCH_3 + O_2 \rightarrow O_2CH_2OCH_3^* \qquad (6c)$$

Reaction 1d is the aforementioned CO bond cleavage reaction,

10.1021/jp9919718 CCC: $19.00
Published on Web 01/26/2000

reaction 6a is the methoxymethyl radical self-reaction, and reactions 6b and 6c are O_2 addition reactions. Reaction 6b results in the formation of ground-state $O_2CH_2OCH_3$ through collisional quenching with a third body, M, while reaction 6c results in formation of excited-state $O_2CH_2OCH_3$*.

The reaction of the methoxymethyl radical with O_2 (reactions 6b and 6c) and the subsequent fate of the methoxymethylperoxy radical, $O_2CH_2OCH_3$, has been the subject of numerous studies. Jenkin et al.[9] examined dimethyl ether degradation pathways in the absence of NO. With this scenario, two methoxymethylperoxy radicals, $O_2CH_2OCH_3$, can combine to yield two methoxymethoxy radicals, OCH_2OCH_3 (reaction 7). The methoxymethoxy radicals can further react with O_2 to yield methyl formate and HO_2 (reaction 8). In Jenkin's investigation, Jenkin et al.[9] found that the rate of reaction 7 varied with pressure and that it also depended on the ratio $[O_2]/[Cl_2]$. This result implied the existence of a secondary chemical reaction. $O_2CH_2OCH_3$ always displayed second-order kinetics, eliminating the possibility of unimolecular bond cleavage reactions. As the relative amount of O_2 increased, the rate constant increased; thus, the intermediate may react with O_2 and ultimately lead to further removal of $O_2CH_2OCH_3$. As the relative amount of Cl_2 increased, the rate constant decreases; thus, the intermediate may react with Cl_2 and ultimately lead to regeneration of $O_2CH_2OCH_3$.

$$O_2CH_2OCH_3 + O_2CH_2OCH_3 \rightarrow OCH_2OCH_3 + OCH_2OCH_3 + O_2 \quad (7)$$

$$OCH_2OCH_3 + O_2 \rightarrow HO_2 + CH_3OC(O)H \quad (8)$$

One possible explanation for these observations is H atom ejection from the methoxymethoxy radical, i.e., reaction 9. Thus, at high concentrations of O_2, hydrogen atoms formed in reaction 9 can react with excess oxygen to yield HO_2 radicals. HO_2 radicals may then further react with methoxymethylperoxy radicals, reactions 10−12, explaining the increased rate of $O_2CH_2OCH_3$ loss at high O_2 concentrations.

$$OCH_2OCH_3 + M \rightarrow CH_3OC(O)H + H + M \quad (9)$$

$$HO_2 + O_2CH_2OCH_3 \rightarrow OH + OCH_2OCH_3 \quad (10)$$

$$HO_2 + O_2CH_2OCH_3 \rightarrow CH_3OCH_2OOH + O_2 \quad (11)$$

$$HO_2 + O_2CH_2OCH_3 \rightarrow CH_3OCOH + H_2O + O_2 \quad (12)$$

At high concentrations of Cl_2, the hydrogen atom emitted in reaction 9 may react with excess chlorine to form hydrochloric acid and additional chlorine radicals. The excess chlorine radical further reacts with dimethyl ether and ultimately produces additional $O_2CH_2OCH_3$, explaining the decrease in rate of $O_2CH_2OCH_3$ loss. A question we intend to address is the possibility of other thermal degradation pathways besides CH bond cleavage in OCH_2OCH_3. CO bond cleavage and other rearrangements may compete.

At low total pressures, significant concentrations of formaldehyde, CH_2O, were detected using FTIR spectroscopy. A possible explanation for this finding is the isomerization of $O_2CH_2OCH_3$ to form CH_2OCH_2OOH via a six-membered transition structure. Formaldehyde can then be formed from the decomposition of CH_2OCH_2OOH to form $2CH_2O$ and the OH radical, reaction 13.[9]

$$O_2CH_2OCH_3^* \rightarrow HO_2CH_2OCH_2 \rightarrow 2CH_2O + OH \quad (13)$$

Sehested et al.[12] in 1996 further investigated the isomerization reaction of methoxymethylperoxy radicals. Once energetic methoxymethylperoxy radicals are formed from reaction 6c ($O_2CH_2OCH_3$*) one of two reaction paths can be followed—collisional quenching to form ground-state $O_2CH_2OCH_3$ or intermolecular rearrangement to form CH_2OCH_2OOH (reaction 13), which may decompose to form two formaldehyde molecules and a hydroxyl radical. For total pressures above about 10 Torr, collisional quenching and formation of ground-state methoxymethylperoxy radicals were found to dominate. Below 10 Torr, the concentration of third bodies is too low for significant collisional quenching. Intermolecular rearrangement and formation of formaldehyde was found to dominate.

All of the previous investigations have studied the degradation of dimethyl ether in the absence of NO. Japar et al.[8] used Cl and OH radical initiated hydrogen abstraction to simulate the reaction of DME with tropospheric OH radical in the presence of NO.

$$O_2CH_2OCH_3 + NO \rightarrow OCH_2OCH_3 + NO_2 \quad (14)$$

Reaction products were determined using FTIR spectroscopy. The production of methyl formate accompanied the loss of dimethyl ether quantitatively. The yield of methyl formate relative to DME loss was found to be 0.90. After the initial hydrogen abstraction from dimethyl ether by the hydroxyl radical, reactions 6b, 14, and 8 were suggested as being responsible for the formation of methyl formate. O_2 abstraction of a hydrogen atom from OCH_2OCH_3 (reaction 8) occurs at the CH bond α to the radical center. The other possibility would be O_2 attack at the β carbon forming OCH_2OCH_2 and ultimately $2CH_2O$. However, no evidence of participation in this degradation channel was found.

The above investigations include only up to the formation of methyl formate. The atmospheric fate of methyl formate is largely undetermined. In addition, the relative thermodynamics of much of the dimethyl ether degradation mechanism is unknown. We present a detailed ab initio investigation into the oxidation of dimethyl ether.

II. Computational Method

All calculations were performed with the GAUSSIAN 94 package of programs.[14] Geometry optimizations for all species were carried out for all structures to better than 0.001 Å for bond lengths and 0.1° for angles. The geometries were fully optimized and, with these geometries, a frequency calculation was performed using the second-order Møller−Plesset (UMP2) level, with restricted wave functions for closed-shell and unrestricted for open-shell systems with all orbitals active using the 6-31G(d) basis set. In addition, G2 and G2MP2 energies were calculated using G2 methodology.[15−17] The total energies are corrected to 0 K by adding the zero-point energy to the predicted total energy. To obtain the energy at 298 K, the thermal energy of each species is added to its total energy instead of the zero-point energy. The reaction enthalpy at 0 or 298 K can then be obtained by use of the corrected energy along with the following equation.

$$\Delta H = \Delta E - \Delta nRT \quad (15)$$

For a reaction with the same number of products as reactants, the change in molecularity, Δn, is zero and $\Delta H = \Delta E$.

To improve the accuracy of the method, isodesmic reactions were used. Isodesmic and isogiric reactions are those in which reactants and products contain the same type of bonds, same

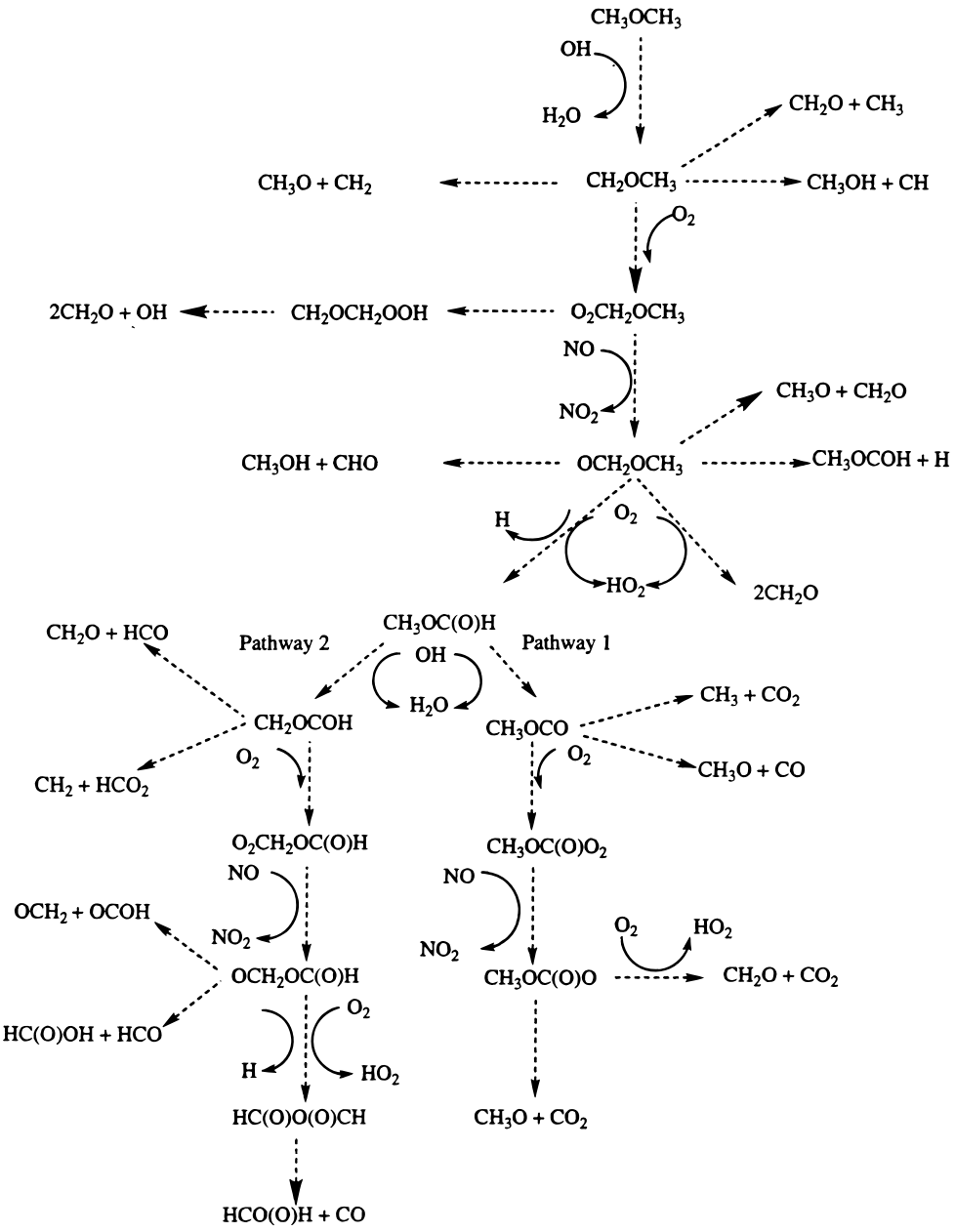

Figure 1. Atmospheric degradation pathways for dimethyl ether and methyl formate.

number of bonds, and the same spin multiplicity.[18] Because of the electronic similarity between the reactants and products, errors in the calculated energy may cancel between them.

For each species, the degree of spin contamination was monitored. For most doublet systems, the $\langle s^2 \rangle$ value did not exceed 0.76. There is, however, one class of reactions for which this condition is not met. The three hydrogen abstraction reactions initiated by molecular oxygen each had $\langle s^2 \rangle$ values in excess of 0.76, which could lead to a deteriorated estimate of the barrier height.

III. Results and Discussions

The complete map of possible degradation pathways is shown in Figure 1.

A. Structures of Closed- and Open-Shell Species Involved in the Oxidation of Dimethyl Ether. As shown in Figure 2a, dimethyl ether exists in C_{2v} symmetry with two equivalent CO bond lengths (1.414 Å) and two distinct hydrogen environments. The two in-plane hydrogens have CH bond lengths of 1.090 Å. The four out-of-plane CH bonds have lengths of 1.099 Å. Table 1 lists the calculated structure along with experimental values from Blukis et al.[19] All calculated values are in reasonable agreement with experimental findings.

The methoxymethyl radical (Figure 2b) displays C_1 symmetry with two differing CO bond lengths. The CO bond length decreases relative to the parent ether from 1.414 to 1.363 Å, while the C′O bond increases in length to 1.424 Å. On the CH_2 group, one hydrogen atom remains in-plane with a dihedral angle of 177.4° and a bond length of 1.081 Å, while the CH‴ bond remains in out-of-plane, having a dihedral angle of 32.4° and a slightly longer bond length of 1.088 Å. An O_2 molecule attaches to the vacant out-of-plane site on CH_2OCH_3, forming $O_2CH_2OCH_3$ (Figure 2c).

Methyl formate adopts C_s symmetry, as illustrated in Figure 2e. Electron diffraction and microwave studies have shown the planar cis form to be more stable than the trans form.[20,21] The

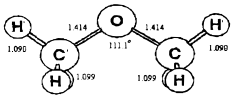

(a) CH_3OCH_3

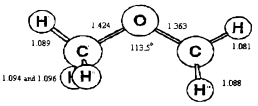

(b) CH_3OCH_2

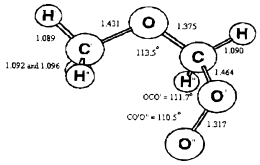

(c) $CH_3OCH_2O_2$

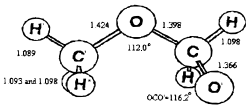

(d) CH_3OCH_2O

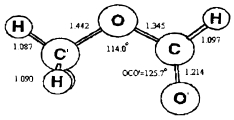

(e) CH_3OCOH

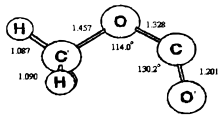

(f) CH_3OCO

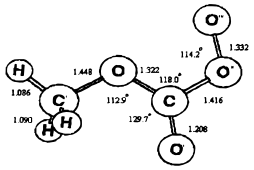

(g) $CH_3OC(O)O_2$

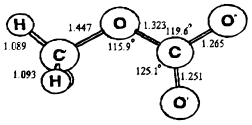

(h) $CH_3OC(O)O$

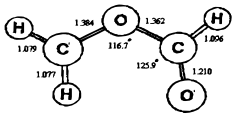

(i) CH_2OCOH

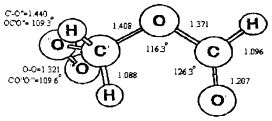

(j) O_2CH_2OCOH

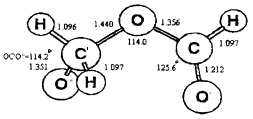

(k) OCH_2OCOH

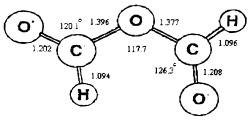

(l) HOCOCOH

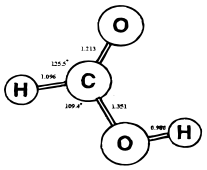

(m) HC(O)OH

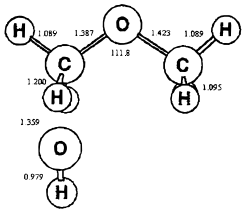

$CH_3OCH_3 + OH \rightarrow CH_3OCH_2 + H_2O$

(n)

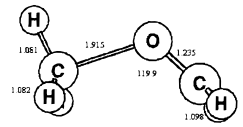

$CH_3OCH_2 \rightarrow CH_3 + CH_2O$

(o)

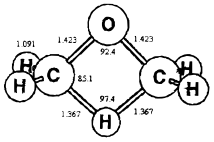

$CH_3OCH_2 \rightarrow CH_3 + CH_2O$

(p)

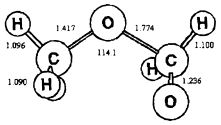

$CH_3OCH_2O \rightarrow CH_3O + CH_2O$

(q)

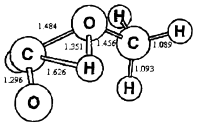

$CH_3OCH_2O \rightarrow CH_3OH + HCO$

(r)

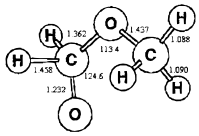

$CH_3OCH_2O \rightarrow CH_3OCOH + H$

(s)

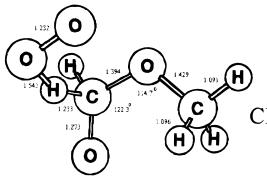

$CH_3OCH_2O + O_2 \rightarrow CH_3OCOH + HO_2$

(t)

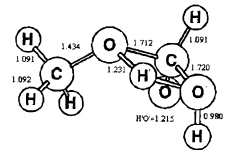

$CH_3OCOH + H_2O \rightarrow CH_3OH + HCO_2H$ (u)

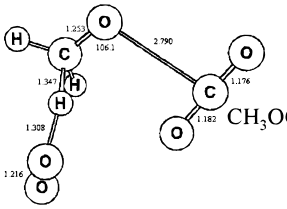

$CH_3OC(O)O + O_2 \rightarrow CH_2O + CO_2 + HO_2$ (aa)

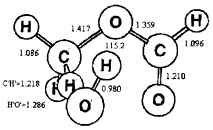

$CH_3OCOH + OH \rightarrow CH_2OCOH + H_2O$ (v)

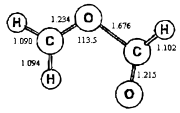

$CH_2OCOH \rightarrow CH_2O + HCO$ (bb)

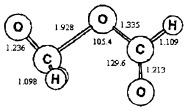

$OCH_2OCOH \rightarrow CH_2O + HC(O)O$ (cc)

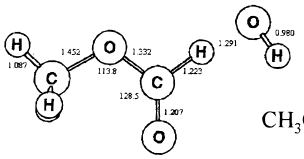

$CH_3OCOH + OH \rightarrow CH_3OCO + H_2O$ (w)

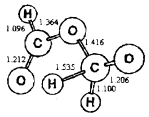

$OCH_2OCOH \rightarrow HOCOCOH + H$ (dd)

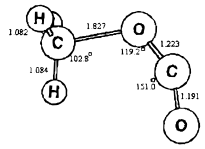

$CH_3OCO \rightarrow CH_3 + CO_2$ (x)

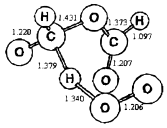

$OCH_2OCOH + O_2 \rightarrow HOCOCOH + HO_2$ (ee)

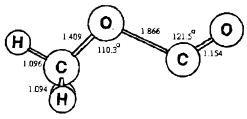

$CH_3OCO \rightarrow CH_3O + CO$ (y)

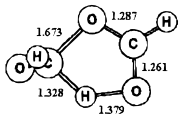

$OCH_2OCOH \rightarrow HCO_2H + HCO$ (ff)

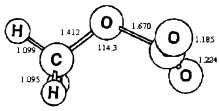

$CH_3OC(O)O \rightarrow CH_3 + CO_2$ (z)

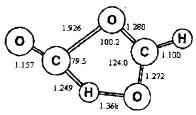

$HOCOCOH \rightarrow HCO_2H + CO$ (gg)

Figure 2. Structures of closed- and open-shell species and transition structures involved in the oxidation of dimethyl ether and methyl formate.

TABLE 1: Structure of Dimethyl Ether[a]

coordinate	MP2/6-31G(d)	expt[b]
CO	1.414	1.410
CH (in-plane)	1.090	1.091
CH (out-of-plane)	1.099	1.100
COC	111.1	111.7
HCO (in-plane)	106.9	107.2
HCO (out-of-plane)	111.5	110.8
HCOC (in-plane)	180.0	180.0
HCOC (out-of-plane)	60.7	

[a] Bond lengths in angstroms, bond angles in degree. [b] Reference 19.

TABLE 2: Structure of Methyl Formate[a]

coordinate	MP2/6-31G(d)	expt[b]
C′O	1.442	1.437
CO	1.345	1.334
CO′	1.214	1.200
CH	1.098	1.101
C′H (in-plane)	1.087	1.086
C′H (out-of-plane)	1.090	
C′OC	114.0	114.8
OCO′	125.7	125.9
OCH	108.1	109.3
OC′H (in-plane)	105.1	
OC′H (out-of-plane)	110.3	
OCOC′	0.0	0.0
HCOC′	180.0	180.0
HC′OC (in-plane)	180.0	180.0
HC′OC (out-of-plane)	60.4	

[a] Bond lengths in angstroms, bond angles in degrees. [b] Reference 20.

energy difference ranges from a low of 1.1 to a high of 9.0 kcal mol^{-1}.[22−28] The two experimental investigations list the enthalpy difference as 2.3 and ≥2.7 kcal mol^{-1}.[26−28] The gauche form of methyl formate represents the barrier height of rotation and is reported to be between 5.5 and 13.1 kcal mol^{-1}.[22−28] Table 2 lists the calculated structure of methyl formate, as well as literature values. As shown in Table 2, our values agree with experimental findings. The ether linkage C′O bond has increased to 1.442 Å, while the opposing CO bond decreases substantially from 1.398 to 1.345 Å. The carbonyl CO′ bond has also decreased to a typical double bond length of 1.214 Å. The oxygen atom orients itself downward, forming a COCO dihedral angle of 0.0°.

Hydrogen abstraction from methyl formate yields the CH_3-OCO radical. As illustrated in Figure 2f, the molecule remains in C_s symmetry, with dihedral angles of COC′H = 180.0° and

TABLE 3: Structure of Formic Acid Anhydride[a]

coordinate	MP2/6-31G(d)	Lundell et al.[b]	exptl[c]
CO′	1.208	1.208	1.195
CO	1.377	1.377	1.364
C′O	1.396	1.396	1.389
C′O″	1.202	1.202	1.184
CH	1.096	1.091	1.096
C′H	1.094	1.089	1.101
OCO′	126.3	126.3	126.1
C′OC	117.8	117.5	117.8
O″C′O	120.1	120.1	120.6
O″C′H	125.3	125.7	
O′CH	127.1	126.8	
O′COC′	0.0	0.0	0.0
COC′O″	180.0	180.0	180.0

[a] Bond lengths in angstroms bond angles in degrees. [b] Reference 30. [c] Reference 29.

C′OCO′ = 0.0. Subsequent reactions with O_2 and NO result in the formation of $CH_3OC(O)O_2$ and $CH_3OC(O)O$, respectively.

Hydrogen abstraction from methyl formate can also result in the formation of CH_2OCOH (Figure 2i). As with dimethyl ether, one of the out-of-plane hydrogens is removed, leaving one hydrogen in more of an in-plane position with a CH bond length of 1.079 Å and a COCH dihedral angle of 169.3°. The out-of-plane hydrogen has a CH bond length of 1.077 Å and a COCH dihedral angle of 16.7. Molecular oxygen addition to CH_2OCOH yields O_2CH_2OCOH (Figure 2j). The forming peroxide C′O″ bond has a bond length of 1.440 Å, while the O″O‴ bond lengthens to 1.321 Å. This alkyl peroxyl radical is reduced to OCH_2OCOH, as shown in Figure 2k.

The structure of formic acid anhydride is shown in Figure 2l. The structure of formic acid has been studied by Vaccani et al.[29] and Lundell et al.[30] The AE (where A and E denote in-plane and out-of-plane formyl groups, respectively) conformer has been found to be the most stable isomer, followed by the AA (+∼8.6 kcal mol^{-1}) conformer, and finally the EE (+∼16.3 kcal mol^{-1}) isomer.[29−31] The AE conformer has both oxygen atoms within the COC plane, both oriented anti with respect to one another. The trans side of the molecule has a carbonyl bond distance of 1.202 Å, an ether linkage CO distance of 1.396 Å, and a CH distance of 1.094 Å. The opposing cis side contains a longer carbonyl bond distance of 1.208 Å, a shorter CO bond distance of 1.377 Å, and a slightly longer CH bond distance of 1.096 Å. The COC angle connecting the two sides is 117.7°. Table 3 reports the structure of formic acid anhydride and compares it with literature values. Our structure is in reasonable agreement with the experimental determination.

The structure of *trans*-formic acid is shown in Figure 2m. The CH bond length is 1.095 Å. The carbonyl CO bond has a bond length of 1.213 Å and makes a 125.5° angle with respect to the CH bond. The CO single bond is 1.351 Å long and makes a 109.4° angle with respect to the CH bond. The OH bond length is 0.98 Å and is oriented trans to the CH bond.

B. Thermochemistry of Closed- and Open-Shell Species Involved in the Oxidation of Dimethyl Ether. The overall reaction mechanism is illustrated in Figure 1. The heat of formation for some of the reactants and products are well-documented in the literature. However, for many of the key intermediates, thermodynamic data do not yet exist. Thus, the second part of this investigation will focus on determining heats of formation for species involved in the oxidation mechanism. A series of isodesmic schemes will be used toward this end. The isodesmic nature of these reactions allows for high-accuracy determinations of the reaction enthalpies. The heat of formation of the species of interest can then be determined using literature values for the remaining species in the reaction. Table 4 lists thermodynamic properties for all species used in isodesmic reactions. Table 5 lists the heat of formation of degradation intermediates, along with the isodesmic reactions used to generate them. Many of the literature values in Table 5 were taken from the work of Curran et al.,[32] who used group additivity methods to estimate the heats of formation of various species involved in the combustion of dimethyl ether. The heats of formation of dimethyl ether and the methoxymethyl radical have been reported in a previous study using the present methodology.[33] Dimethyl ether was found to have a heat formation at 298 K of −44.0 kcal mol^{-1}, while the methoxymethyl radical was found to have a heat of formation of 0.9 kcal mol^{-1}. The value for dimethyl ether is in agreement with literature values, while that for the methoxymethyl radical was found to disagree substantially.[33]

TABLE 4: Known Thermodynamic Constants for Species Involved in Isodesmic Reactions[a]

species	$\Delta H_{f,0K}$	$\Delta H_{f,298K}$	ref
H_2O	−57.10 ±.01	−57.80 ±.01	*b*
OH	9.2 ± 0.3	9.3 ± 0.3	*b*
$CH_2(^3B_1)$	93.6 ± 0.6	93.7 ± 0.6	*b*
CH_4	−16.0 ± 0.1	−17.9 ± 0.1	*b*
CH_3	35.8 ± 0.2	35.0 ± 0.1	*b*
CH_2O	−25.1 ± 1.5	−26.0 ±.1	*b*
HCO	9.0 + 0.2	10.0 + 0.2	*b*
HC(O)OH	−88.7	−90.5+0.1	*b*
CH_3OH	−45.4 ± 0.1	−48.0 ± 0.1	*b*
CH_3OCH_3	−39.7 ± 0.1	−44 ± 0.1	*b*
CH_2OCH_3	4.2	0.9	*d*
HOO	3.5 ± 0.5	2.8 ± 0.5	*e*
H_2O_2	−31.0	−32.5	*b*
CH_3O		4.1 ± 0.9	*b*
CH_3O_2		2.2	*c*
CO_2	−94.0	−94.1	*b*
CO	−27.2	−26.4	*b*
CH3OOH		−31.3	*f*
H	51.6	52.1	*b*
HCO_2	−28.6	−31.0	*g*
CH_3OCOH		−85.0 ± 0.2	*b*

[a] All values in kcal mol^{-1}. [b] Curtiss, L. A.; Raghavachari, K.; Redfern, P. C.; Pople J. A. *J. Chem. Phys*. **1997**, *106* (3), 1063. [c] Lay, T. H.; Bozzelli, J. W. *J. Phys. Chem. A* **1997**, *101*, 9505. [d] Good, D. A.; Francisco, J. S. *Chem. Phys. Lett*. **1997**, *266*, 512. [e] Bauschlicher, C. W., Jr.; Partridge, H. *Chem. Phys. Lett*. **1993**, *208*, 241. [f] JANAF Thermochemical tables. *J. Phys. Chem. Ref. Data* **1985**, No. 14, Suppl. 1. [g] Langford, S. R.; Batten, A. D.; Kono, M.; Ashfold, N. R. *J. Chem. Soc., Faraday Trans*. **1997**, *93* (21), 3757−3764.

The methoxymethoxy radical was found to have a heat of formation of −35.9 kcal mol^{-1}. The literature value of −34.5 kcal mol^{-1} deviates from our value by about 4%. As shown in Table 5, all reactions are dependent on the heat of formation of the CH_3O radical. The heat of formation of the methoxy radical has a relatively large error associated with it of 0.9 kcal mol^{-1}, or 22%.[34] The third reaction of the reaction set also uses the controversial value for the heat of formation of the CH_3OCH_2 radical. As shown, the third reaction is in agreement with the first two reactions, lending support for the 0.9 kcal mol^{-1} value used for the heat of formation of CH_3OCH_2.[33]

The methoxymethylperoxy, $O_2CH_2OCH_3$, radical has a heat of formation of −39.4 kcal mol^{-1}. The literature value of −35.9 kcal mol^{-1} deviates by a relatively large 9.7%. The first three reactions involve methoxy and methylperoxy radicals, both of which have relatively high uncertainties in their heats of formation. The ΔH_f^{298} of the CH_3O_2 radical was determined to be −5.5 ± 1.0 kcal mol^{-1}, as measured by Kondo et al.[35] The

TABLE 5: Isodesmic Reaction Schemes for Closed- and Open-Shell Species Involved in Dimethyl Ether Atmospheric Oxidation

species	isodesmic reaction	ΔH_f^{298} [a]	lit. (298 K)
OCH_2OCH_3	$OCH_2OCH_3 + CH_4 \rightarrow CH_3O + CH_3OCH_3$	−35.9	
	$OCH_2OCH_3 + CH_2O \rightarrow CH_3O + CH_3OCOH$	−35.9	
	$OCH_2OCH_3 + CH_3 \rightarrow CH_3O + CH_2OCH_3$	−36.0	
	av	−35.9	−34.5
$O_2CH_2OCH_3$	$O_2CH_2OCH_3 + OH + CH_4 \rightarrow CH_3O + CH_3OCH_3 + HO_2$	−40.2	
	$O_2CH_2OCH_3 + CH_3O \rightarrow CH_3O_2 + CH_3OCH_2O$	−38.9	
	$O_2CH_2OCH_3 + CH_4 \rightarrow CH_3O_2 + CH_3OCH_3$	−38.8	
	$O_2CH_2OCH_3 + OH \rightarrow OCH_2OCH_3 + HO_2$	−39.5	
	av	−39.4	−35.9
CH_2OCH_2OOH	$CH_2OCH_2OOH + 2CH_4 \rightarrow CH_3 + CH_3OOH + CH_3OCH_3$	−24.0	
	$CH_2OCH_2OOH + CH_4 + OH \rightarrow H_2O_2 + CH_3 + CH_3OCH_2O$	−25.4	
	$CH_2OCH_2OOH + CH_4 + HO_2 \rightarrow H_2O_2 + CH_3 + CH_3OCH_2O_2$	−24.8	
	av	−24.7	−26.1
CH_3OCOH	$CH_3OCOH + CH_2O \rightarrow CH_3OCH_3 + CO_2$	−86.5	
	$CH_3OCOH + CH_4 \rightarrow CH_3OCH_3 + CH_2O$	−85.0	
	$CH_3OCOH + CH_3 \rightarrow CH_3OCH_3 + CHO$	−85.7	
	av	−85.7	−85.0
CH_3OCO	$CH_3OCO + CH_4 \rightarrow CH_3OCOH + CH_3$	−37.1	
	$CH_3OCO + CH_4 \rightarrow CH_3OCH_3 + CHO$	−37.7	
	$CH_3OCO + CH_2O \rightarrow CH_3OCOH + CHO$	−37.7	
	av	−37.5	-
CH_2OCOH	$CH_2OCOH + CH_4 \rightarrow CH_3OCH_3 + CHO$	−36.7	
	$CH_2OCOH + CH_4 \rightarrow CH_3OCOH + CH_3$	−36.0	
	$CH_2OCOH + CH_2O \rightarrow CH_3OCOH + CHO$	−36.7	
	av	−36.5	-
$CH_3OC(O)O_2$	$CH_3OC(O)O_2 + CH_4 \rightarrow CH_3O_2 + CH_3OCOH$	−73.5	
	$CH_3OC(O)O_2 + 2CH_4 \rightarrow CH_3O_2 + CH_3OCH_3 + CH_2O$	−73.7	
	$CH_3OC(O)O_2 + OH \rightarrow HO_2 + CH_3OC(O)O$	−74.2	
	$CH_3OC(O)O_2 + H_2O \rightarrow H_2O_2 + CH_3OC(O)O$	−73.4	
	av	−73.7	-
O_2CH_2OCOH	$O_2CH_2OCOH + CH_4 \rightarrow CH_3O_2 + CH_3OCOH$	−74.2	
	$O_2CH_2OCOH + 2CH_4 \rightarrow CH_3O_2 + CH_3OCH_3 + CH_2O$	−74.4	
	$O_2CH_2OCOH + OH \rightarrow HO_2 + OCH_2OCOH$	−74.3	
	$O_2CH_2OCOH + H_2O \rightarrow H_2O_2 + OCH_2OCOH$	−73.6	
	av	−74.1	-
$CH_3OC(O)O$	$CH_3OC(O)O + CH_4 \rightarrow CH_3OCOH + CH_3O$	−82.0	
	$CH_3OC(O)O + H_2O + CH_4 \rightarrow CH_3OCH_3 + OH + HC(O)OH$	−81.2	
	av	−81.6	-
OCH_2OCOH	$OCH_2OCOH + CH_4 \rightarrow CH_3OCOH + CH_3O$	−73.8	
	$OCH_2OCOH + CH_4 + H_2O \rightarrow OH + CH_3OCOH + CH_3OH$	−71.8	
	av	−72.8	−75.5
HOCOCOH	$HOCOCOH + 2CH_2O \rightarrow CH_3OCH_3 + 2CO_2$	−115.0	
	$HOCOCOH + 2CH_4 \rightarrow CH_3OCH_3 + 2CH_2O$	−112.0	
	$HOCOCOH + CH_2O \rightarrow CH_3OCOH + CO_2$	−113.5	-
	av	−113.5	
HC(O)OH	$HC(O)OH + CH_3 \rightarrow CH_3OH + HCO$	−90.0	
	$HC(O)OH + CH_4 \rightarrow CH_3OH + CH_2O$	−89.3	
	av	−89.7	−90.5

[a] Using values calculated at G2 level of theory (in kcal mol^{-1}).

heat of formation is later remeasured by Slagel et al.[36] (2.41 ± 0.80 kcal mol^{-1}) and then revised by Knyazev et al.[37] (2.15 ± 1.22 kcal mol^{-1}). Finally, an ab initio investigation by Jungkamp et al.[38] finds a ΔH_f^{298} of 2.24 kcal mol^{-1} at the G2(RCC) level of theory. A value of $\Delta H_f^{298} = 2.2$ kcal mol^{-1} was used in this study.[39] The fourth reaction scheme incorporates the previously determined heat of formation for the methoxymethoxy radical, along with hydroxyl and hydroperoxyl radicals. The fourth reaction is in agreement with the first three, lending credibility to the calculated heats of formation for both the methoxymethoxy radical and the methoxymethylperoxy radical.

CH_2OCH_2OOH was found to have a heat of formation of −24.7 kcal mol^{-1}. The literature value from Curran et al.[32] is −26.6 kcal mol^{-1}, which deviates from the present value by about 7%. The isodesmic schemes used to calculate the heat of formation at 298 K are listed in Table 5. The first reaction uses established enthalpy values for methane, the methyl radical,

methyl hydroperoxide, and dimethyl ether. The second and third reactions incorporate enthalpy data from methoxymethoxy and methoxymethylperoxy radicals. The consistency between the three reactions suggests reasonable values for methoxymethoxy and methoxymethylperoxy radicals. CH_2OCH_2OOH lies approximately 14.7 kcal mol^{-1} higher in energy than $CH_3OCH_2O_2$. At the MP2/6-31G(d) level of theory, $T\Delta S$ is calculated to be 0.51 kcal mol^{-1}. With these values for ΔS and ΔH, an equilibrium constant for the conversion of $CH_3OCH_2O_2$ to CH_2OCH_2OOH is estimated to be on the order of 10^{-11} at 298 K. Sehested et al.[12] observed evidence (the formation of CH_2O) for the conversion reaction only at low total pressures. The rate constant for reaction 6c, k_{6c}, was compared to reaction 16. At

$$CH_3OCH_2 + Cl_2 \rightarrow CH_3OCH_2Cl + Cl \qquad (16)$$

the high- and low-pressure limits, Sehested et al.[12] found k_{6b}/k_{16} to be 0.108 and 1.97×10^{-19} cm^3 molecule^{-1}, respectively. At the low-pressure limit, the rate constant for consecutive reactions 6c and 13, $k_{6c,13}$ was compared to k_{16}. $k_{6c,13}/k_{16}$ was determined to be 0.063. In addition, a pressure independent estimate for k_{16} was calculated to be 1.0×10^{-10} cm^3 molecule^{-1} s^{-1}. This value for k_{16} results in the following rate data: $k_{6b,lowpressure} = 2.0 \times 10^{-29}$ cm^6 molecule^{-2} s^{-1}, $k_{6b,highpressure} = 1.1 \times 10^{-11}$ cm^3 molecule^{-1} s^{-1}, and $k_{6c,13} = 6.3 \times 10^{-12}$ cm^3 molecule^{-1} s^{-1}. Thus, under atmospheric conditions where significant concentrations of third bodies exist, formation of ground-state methoxy methoxy radicals would be expected to dominate.

Sehested et al.[13] revisited this work using the pulse radiolysis technique. In this investigation, the following rate data were obtained: $k_{6b,lowpressure} = 9.4 \times 10^{-30}$ cm^6 molecule^{-2} s^{-1}, $k_{6b,highpressure} = 1.14 \times 10^{-11}$ cm^3 molecule^{-1} s^{-1}, and $k_{6c,13lowpressure} = 6.0 \times 10^{-12}$ cm^3 molecule^{-1} s^{-1}. Independently, Maricq et al.[40] determined nearly identical values for these rates. Their investigation finds $k_{6b,lowpressure} = 2.6 \times 10^{-29}$ cm^6 molecule^{-2} s^{-1}, $k_{6b,highpressure} = 1.1 \times 10^{-11}$ cm^3 molecule^{-1} s^{-1}, and $k_{6c,13lowpressure} = 6.0 \times 10^{-12}$ cm^3 molecule^{-1} s^{-1}. The values in these studies are in reasonable agreement with the previous investigation.

At low pressures, the excited state of $CH_3OCH_2O_2$ is not collisionally quenched to the ground state, and the high-energy $CH_3OCH_2O_2$* radical rearranges to CH_2OCH_2OOH. However, under both atmospheric and combustion conditions where concentrations of third bodies are relatively high, the $CH_3OCH_2O_2$ radical will likely be quenched to the ground state. In this case, our calculations and the work of Sehested et al.[12,13] suggest that conversion to CH_2OCH_2OOH is improbable.

Methyl formate was calculated to have a heat of formation of -85.7 kcal mol^{-1}. The well-established heat of formation of -85.0 kcal mol^{-1} deviates by less than 1%. As indicated by its low enthalpy of formation, methyl formate is a very stable species as compared to its precursors.

Methyl formate undergoes hydrogen abstraction reactions forming CH_3OCO and/or CH_2OCOH. Heats of formation for neither species has been found in the literature. CH_3OCO is found to be slightly more stable than CH_2OCOH by about 1 kcal mol^{-1}. CH_3OCO has a ΔH_f^{298} of -37.5 kcal mol^{-1}, while CH_2OCOH has a ΔH_f^{298} of -36.5 kcal mol^{-1}. Both isodesmic reaction sets use the same species (CH_4, CH_3, CH_2O, and HCO) in their respective reaction sets.

O_2 addition to CH_3OCO and CH_2OCOH yields $CH_3OC(O)O_2$ and O_2CH_2OCOH, respectively, having heats of formation at 298 K of -73.7 and -74.1 kcal mol^{-1}, respectively. For both species, the first two reactions in the set involve the conversion of methane to the CH_3O_2 radical. The latter two reactions in each set incorporate the formation of HO_2 radicals from either the OH radical or water. In addition, the latter two reactions use the heat of formation of CH_3OCOO and OCH_2OCOH, respectively, which are discussed in the preceding paragraph. As shown in Table 5, all four reactions in each set are consistent, lending credibility to the calculated values.

CH_3OCOO and OCH_2OCOH are possible degradation intermediates. Unlike the previous two comparisons, there is a much larger difference between the heats of formation for the two species. CH_3OCOO has a heat of formation of -81.6 kcal mol^{-1}, while OCH_2OCOH has a heat of formation of -72.8 kcal mol^{-1}. The literature value of -75.5 kcal mol^{-1} deviates by 3.6%.

Formic acid anhydride is the most stable species in the proposed reaction scheme and has a heat of formation of -113.5 kcal mol^{-1}. No literature value for the heat of formation for this species has been found. Formic acid was found to have a heat of formation at 298 K of -89.7 kcal mol^{-1}. This value is in agreement with the well-established literature value of -90.5 kcal mol^{-1}. A deviation of less than 1% exists.

C. Reaction Pathways for Dimethyl Ether Oxidation. *1. CH_3OCH_3.* The first step in the oxidation of dimethyl ether is reaction with OH radicals. This reaction is illustrated in Figure 2n.[41] The longer out-of-plane CH bonds are preferred for abstraction as the hydroxyl radical approaches. In the transition structure, the CH bond increases in length to 1.200 Å and is ultimately removed from dimethyl ether. As the hydroxyl radical approaches, the forming OH bond is found to have a length of 1.359 Å in the transition structure.

The enthalpy of reaction and barrier height is also listed in Figure 3. The enthalpy of reaction is predicted to be -21.6 kcal mol^{-1}, using the G2 level of theory, and -22.4 kcal mol^{-1} at the G2(MP2) level of theory. Good et al.[33] determined a heat of formation for the methoxymethyl radical of 0.9 kcal mol^{-1} at 298 K. Using literature values for the heats of formation of dimethyl ether (-44.0 kcal mol^{-1}), water (-57.8 kcal mol^{-1}), and the hydroxyl radical (9.3 kcal mol^{-1}), a heat of reaction of -22.2 kcal mol^{-1} is derived. Good et al. predicted a reaction enthalpy of -22.5 kcal mol^{-1} using calculated CH bond dissociation enthalpies for dimethyl ether.[42] All three determinations are in reasonable agreement with each other.

The barrier height for hydrogen abstraction is predicted to be 0.1 and 0.2 kcal mol^{-1} at the G2 and G2(MP2) levels of theory, respectively. Experimental determinations by Wallington et al.[43,44] and Trully et al.[45] find a barrier height between 0.6 and 0.8 kcal mol^{-1}. The rate of this reaction has been studied by Perry et al.,[46] Trully et al.,[45] and Wallington et al.[43,44] An average activation energy of 0.7 kcal mol^{-1} has been reported. At 298 K, the average rate constant for this reaction is approximately 2.8×10^{-12} cm^3 molecule^{-1} s^{-1}. Using experimental rate data and 2D chemical transport models, Good et al.[47] determined an atmospheric lifetime of 5.1 days for the dimethyl ether reaction with the hydroxyl radical. Atmospheric degradation of dimethyl ether was predicted to occur solely in the troposphere. From a set of 148 molecules, calculated heats of formation using G2 theory were found to have an average absolute deviation of 1.58 kcal mol^{-1} from experiment. G2(MP2) values were found to deviate from experiment by over 2.04 kcal mol^{-1}.[34] The activation energy calculated for the dimethyl ether/hydroxyl radical reaction is within experimental error, given the above estimated G2 and G2(MP2) errors.

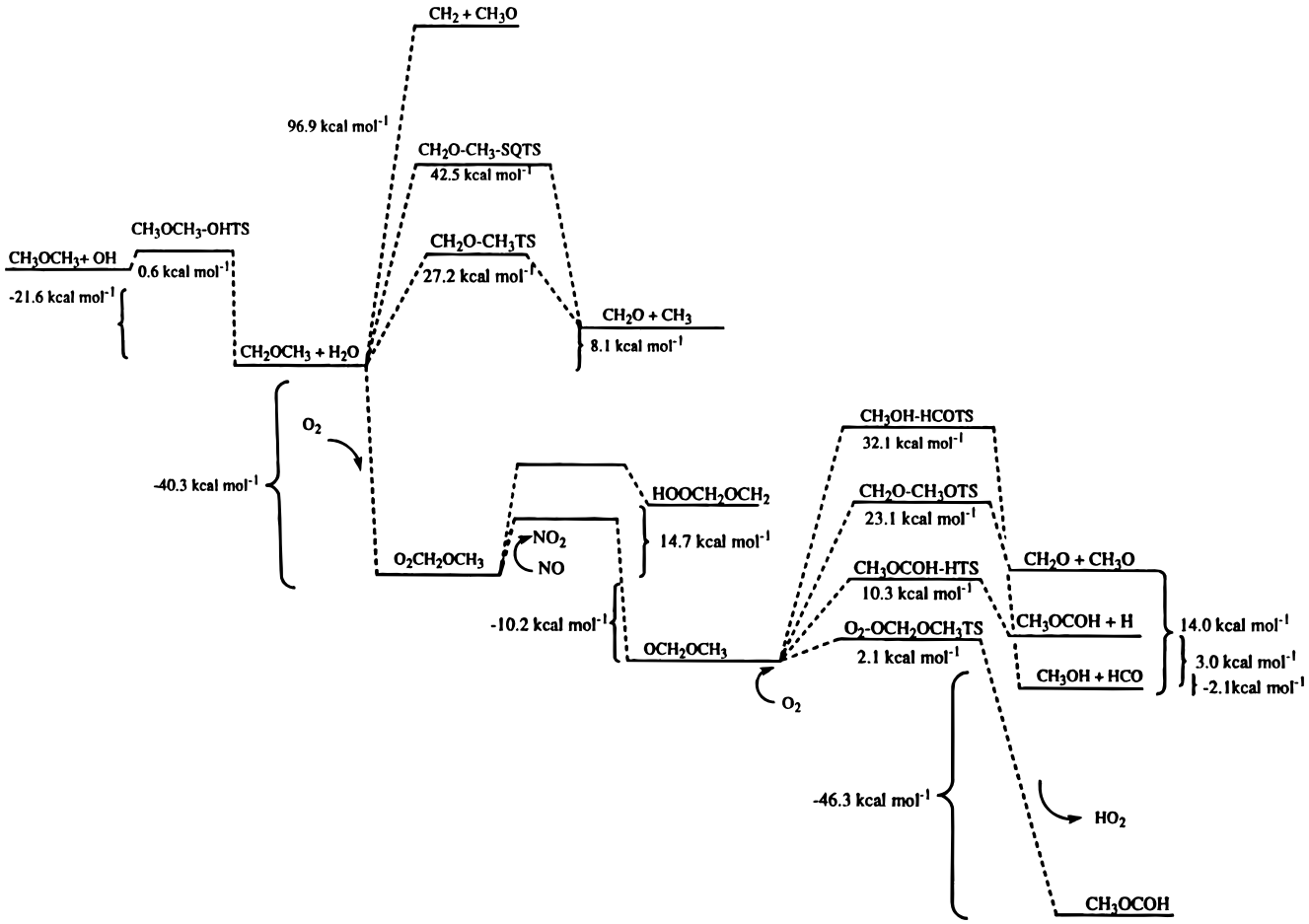

Figure 3. Energetics of the degradation pathways for dimethyl ether.

2. CH_2OCH_3. The formed methoxymethyl radical, CH_2OCH_3, may participate in the following reaction channels.

$$CH_2OCH_3 + M \rightarrow M + CH_2 + CH_3O \quad (17)$$

$$M + CH_2OCH_3 \rightarrow CH_2O + CH_3 + M \quad (1d)$$

$$CH_2OCH_3 \rightarrow CH_2O + CH_3 \quad (18)$$

$$CH_2OCH_3 \rightarrow CH_3OH + CH \quad (19)$$

$$CH_2OCH_3 + O_2 \rightarrow O_2CH_2OCH_3 \quad (6b)$$

Reaction 17 is a CO bond cleavage reaction forming CH_2 and the CH_3O radical. Using the heats of formations from Tables 4 and 5, an enthalpy of reaction of 96.9 kcal mol^{-1} was calculated. Using G2 and G2(MP2) levels of theory, heats of formation of 99.9 and 100.8 kcal mol^{-1} were determined. No higher energy barrier was found for this reaction. Several points calculated along the reaction coordinate indicate a gradual progression toward products.

Reaction 1d is also a CO bond cleavage reaction forming formaldehyde, CH_2O, and the methyl radical, CH_3. The reaction is only slightly endothermic, with a reaction enthalpy of 8.1 kcal mol^{-1}. A reaction barrier of 27.2 kcal mol^{-1} was found in this work, while Curran et al.[32] estimate a reaction barrier of 25.5 kcal mol^{-1}. The energetics of this reaction are illustrated in Figure 3. In the transition structure (Figure 2o), the CO bond adjacent to the CH_3 functional group increases from 1.420 Å in CH_2OCH_3 to 1.915 Å in the transition structure. The CH_2 functional group in CH_2OCH_3 is oriented parallel to the COC plane. As the CH_2O functional group pulls away, however, the CH_2 functional group reorients itself perpendicular to the COC plane.

Reaction 18 produces formaldehyde and the methyl radical just as reaction 1d. Reaction 18, however, proceeds through a four-centered transition structure, as shown in Figure 2p. While the thermodynamics for reaction 18 are identical to that of reaction 1d, the barrier height is much larger. The barrier height for reaction 18 is 42.5 kcal mol^{-1}, as compared to the 27.2 kcal mol^{-1} barrier height for reaction 1d. The transition structure structure has C_{2v} symmetry, as illustrated in Figure 2p. The two CO bonds are 1.423 Å long. The shared hydrogen atom has CH bond lengths of 1.367 Å.

Reaction 19 involves hydrogen transfer from carbon to oxygen via a three-ring transition structure. The heat of reaction for this reaction is 91.7 kcal mol^{-1}. The unfavorable thermodynamics suggest that this channel is probably unimportant, even under combustion conditions.

Reaction 6b is an addition reaction involving oxygen. In reaction 5, an out-of-plane hydrogen is abstracted to form the methoxymethyl radical. In reaction 6b, O_2 adds to this vacant out-of-plane site. As illustrated in Figure 3, the energetics of this reaction are quite favorable. A heat of reaction of −40.3 kcal mol^{-1} was determined using calculated heats of formation, while reaction enthalpies of −42.1 and −42.9 were determined at G2 and G2(MP2) levels of theory, respectively. The bimolecular addition of O_2 to the methoxymethyl radical has no barrier associated with it. Table 6 summarizes the results of the possible CH_2OCH_3 reaction channels.

TABLE 6: Reaction pathways for CH_2OCH_3[a]

	reaction enthalpy[b]			activation barrier	
reaction	G2	G2(MP2)	heat of formation	G2	G2(MP2)
$CH_2OCH_3 \rightarrow CH_2 + CH_3O$	106.4	107.1	96.9		
$CH_2OCH_3 \rightarrow CH + CH_3OH$	92.7	92.6	93.6		
$CH_2OCH_3 \rightarrow CH_2O + CH_3$	7.5	7.6	8.1	27.2	27.5
$CH_2OCH_3 \rightarrow CH_2O + CH_3$	7.5	7.6	8.1	42.5	42.5
$O_2 + CH_2OCH_3 \rightarrow O_2CH_2OCH_3$	−42.2	−42.9	−40.3	no barrier	no barrier

[a] All values in kcal mol^{-1}. [b] Reaction enthalpy computed at 298 K.

3. $O_2CH_2OCH_3$. The $O_2CH_2OCH_3$ radical formed at this point can participate in two major reaction channels. As discussed by Wallington et al.,[10] $O_2CH_2OCH_3$ may undergo molecular rearrangement to form CH_2OCH_2OOH, reaction 13a. This

$$O_2CH_2OCH_3 \rightarrow CH_2OCH_2OOH \quad (13a)$$

$$CH_2OCH_2OOH \rightarrow 2CH_2O + OH \quad (13b)$$

$$O_2CH_2OCH_3 + NO \rightarrow OCH_2OCH_3 + NO_2 \quad (14)$$

intermediate may then decompose to form two formaldehyde molecules and the hydroxyl radical, reaction 13b. The formation of CH_2OCH_2OOH is endothermic by 14.7 kcal mol^{-1}. The following dissociation into formaldehyde is exothermic by −18.0 kcal mol^{-1}. The net reaction of converting the methoxymethylperoxy radical into formaldehyde and the hydroxyl radical is exothermic by −3.3 kcal mol^{-1}.

Under atmospheric conditions, reaction of the methoxymethylperoxy radical with NO forming the methoxymethoxy radical and NO_2 is the expected principal reaction channel, reaction 14. Langer et al.[11] studied the kinetics of reaction 14 using the pulse radiolysis-UV absorption technique. By monitoring the increase in absorption at 400 nm, attributed to the formation of the NO_2 radicals, the rate of this reaction was determined. The rate for this reaction is 9.1×10^{-12} cm^3 molecule^{-1} s^{-1}. This rate is over 6 times faster than the methoxymethylperoxy self-reaction (reaction 7) studied by Jenkin et al. ($k = 1.5 \times 10^{-12}$ cm^3 molecule^{-1} s^{-1}). Under atmospheric conditions, NO concentrations are much higher than those of the methoxymethylperoxy radical. Therefore, methoxymethylperoxy reaction with NO will dominate over the self-reaction, supporting the mechanism put forth by Japar et al.[8] This step is exothermic by −15.9 kcal mol^{-1}, while the first step in the rearrangement reaction was endothermic by 14.7 kcal mol^{-1}.

4. OCH_2OCH_3. The methoxymethoxy radical formed in reaction 14 may participate in the following reaction channels.

$$OCH_2OCH_3 \rightarrow CH_2O + CH_3O \quad (20)$$

$$OCH_2OCH_3 \rightarrow CH_3OH + CHO \quad (21)$$

$$OCH_2OCH_3 \rightarrow H + CH_3OCOH \quad (9)$$

$$OCH_2OCH_3 + O_2 \rightarrow CH_3OCOH + HO_2 \quad (8)$$

Reaction 20 is a unimolecular CO bond fission reaction, producing formaldehyde and the methoxy radical. Figure 2q shows that the rupturing CO bond in OCH_2OCH_3 gradually lengthens from 1.399 to 1.774 Å as reactants proceed to the transition structure. The thermodynamics and kinetics of this reaction are illustrated in Figure 3. The reaction is endothermic by about 14.0 kcal mol^{-1} and has an activation barrier of over 23.1 kcal mol^{-1}.

Reaction 21 is a rearrangement reaction in which a hydrogen atom attached to the carbonyl carbon atom shifts to the central oxygen atom, forming methanol and the HCO radical (Figure 2r). In the transition structure, this hydrogen is partially bonded to both carbon and oxygen. The reaction is exothermic by −2.1 kcal mol^{-1} and has an activation barrier of 32.1 kcal mol^{-1}.

Figure 2s depicts reaction 9, which is the hydrogen atom ejection reaction discussed by Jenkin et al.[9] The fracturing CH bond increases from 1.097 to 1.458 Å in the transition structure. The reaction is slightly endothermic, having a reaction enthalpy of only 3.0 kcal mol^{-1}. The barrier height is a modest 10.3 kcal mol^{-1}.

Reaction 8 is an abstraction reaction in which O_2 abstracts a hydrogen atom from the methoxymethoxy radical to form methyl formate and the hydroperoxy radical, HO_2 (Figure 2t). The thermodynamics and kinetics are depicted in Figure 3. The reaction is very exothermic, having a reaction enthalpy of −46.3 kcal mol^{-1}. The activation energy is a modest 2.1 kcal mol^{-1}. The $\langle s^2 \rangle$ value is found to be 0.78, slightly above the expected 0.75 value typical of singlet systems. Of the reactions listed above, reactions 8 and 9 are the most favored. This conclusion is supported by Jenkin's investigation, in which methyl formate was found to be formed almost exclusively. The possible reactions for OCH_2OCH_3 are summarized in Table 7.

5. Oxidation and Hydrolysis of Methyl Formate. There are three main reaction channels that are of atmospheric interest in which methyl formate may participate.

$$CH_3OCOH + OH \rightarrow CH_3OCO + H_2O \quad (22)$$

$$CH_3OCOH + OH \rightarrow CH_2OCOH + H_2O \quad (23)$$

$$CH_3OCOH + H_2O \rightarrow CH_3OH + HC(O)OH \quad (4)$$

The first two reactions are hydrogen abstraction reactions involving the tropospheric hydroxyl radical, while the third reaction is a hydrolysis reaction forming methanol and formic acid. Reaction 22 is illustrated in Figure 2w. In the transition structure, the approaching hydroxyl radical approaches the carbonyl hydrogen. The CH bond lengthens to 1.223 Å in length. The forming OH bond decreases to 1.291 Å and eventually to 0.969 Å in the departing water molecule. Reaction 23 is illustrated in Figure 2v. In the transition structure, the hydroxyl radical approaches one of the two out-of-plane hydrogens. The CH bond lengthens to 1.218 Å, while the forming OH bond decreases to 1.286 Å, and eventually to 0.969 Å, in the departing water molecule. The two hydrogen abstraction reactions were found to have similar thermodynamic and kinetic properties. Reaction 22 has an activation energy of 2.3 kcal mol^{-1} and a reaction enthalpy of −18.6 kcal mol^{-1} (Figure 4a). Reaction 23 has a barrier height of 3.8 kcal mol^{-1} and a reaction enthalpy of −17.5 kcal mol^{-1} (Figure 4b). Reaction 22 is slightly favored, both in its barrier to reaction and in reaction enthalpy. However, the hydroxyl radical is 3 times more likely to collide with the methyl group hydrogens than with the carbonyl hydrogen. Le Calve et al.[48] measured an activation energy of roughly 1 kcal mol^{-1} for the reaction of methyl formate with the hydroxyl

TABLE 7: Reaction Pathways for OCH_2OCH_3[a]

	reaction enthalpy[b]			activation barrier	
reaction	G2	G2(MP2)	heat of formation	G2	G2(MP2)
$OCH_2OCH_3 \rightarrow CH_2O + CH_3O$	13.6	13.5	14.0	23.1	23.2
$OCH_2OCH_3 \rightarrow CH_3OH + CHO$	−3.3	−3.9	−2.1	32.1	31.4
$OCH_2OCH_3 \rightarrow CH_3OCOH + H$	−1.0	−1.6	3.0	10.3	10.1
$O_2 + OCH_2OCH_3 \rightarrow CH_3OCOH + HO_2$	−50.9	−52.1	−46.3		2.1

[a] All values in kcal mol^{-1}. [b] Reaction enthalpy computed at 298 K.

radical. Our determination is in reasonable agreement with this value considering the estimated errors associated with the G2 methodology, as mentioned previously.

Reaction 24 is a hydrolysis reaction that forms methanol and formic acid. The reaction is illustrated in Figure 2u. In the transition structure, the oxygen atom of the water molecule approaches the carbonyl carbon to within 1.720 Å. Simultaneously, this carbonyl carbon pulls away from the CH_3O group to a distance of 1.712 Å. One of the H atoms of the water molecule begins to dissociate while associating with the oxygen atom of the CH_3O group. The dissociating OH bond in the water molecule is 1.215 Å, while the forming OH bond in methanol is 1.231 Å. The activation energy is 45.0 kcal mol^{-1}. The reaction enthalpy is a slightly endothermic 5.0 kcal mol^{-1} at the G2 level of theory, or 4.3 kcal mol^{-1} using individual heats of formation. In addition to being endothermic, the entropy change of the hydrolysis reaction is calculated to be $\Delta S = 3.4 \times 10^{-3}$ J mol^{-1} K^{-1}. Thus, at 298 K, the equilibrium constant is on the order of 10^{-3}. A temperature of over 1000 °C is required to shift the equilibrium to products. Under combustion conditions, this scenario is possible and reaction 24 may compete. The two hydrogen abstraction reactions are energetically favored and faster; however, water is a major product in combustion reactions and is orders of magnitude more concentrated (10^{17} molecules cm^{-3}) than the hydroxyl radical (10^6 molecules cm^{-3}) in the ambient atmosphere. Table 8 summarizes the energetics of the above three reactions.

6. CH_3OCO. CH_3OCO can participate in the following three reaction mechanisms:

$$CH_3OCO \rightarrow CH_3 + CO_2 \quad (25)$$

$$CH_3OCO \rightarrow CH_3O + CO \quad (26)$$

$$CH_3OCO + O_2 \rightarrow CH_3OC(O)O_2 \quad (27)$$

Reaction 25 is a simple CO bond cleavage reaction forming carbon dioxide and the methyl radical. The reaction is illustrated in Figure 2x. The reaction is exothermic by −21.6 kcal mol^{-1} and has an activation barrier of 14.7 kcal mol^{-1} (Figure 4a).

Reaction 26 is also a simple CO cleavage reaction, forming CH_3O and carbon monoxide. The transition structure shown in Figure 2y illustrates the cleaving CO bond increasing to 1.866 Å. The COCO dihedral angle changes substantially from 0.0° to 180.0°. The carbonyl CO bond decreases from 1.201 to 1.150 Å as the triple bond of carbon monoxide forms. The reaction illustrated in Figure 4a is endothermic by 15.2 kcal mol^{-1} and has an activation barrier of 21.8 kcal mol^{-1}.

Reaction 27 is a bimolecular addition reaction forming $CH_3OC(O)O_2$. The reaction illustrated in Figure 4a proceeds without barrier and is exothermic by −36.4 kcal mol^{-1}. The structure of $CH_3OC(O)O_2$ is shown in Figure 2g and was described previously. This reaction is the most favored of the three possible degradation pathways available to the CH_3OCO radical. Under high-pressure conditions, O_2 addition reactions typically have rate constants[49] on the order of 10^{-12} cm^3 $molecule^{-1}$ s^{-1}. In the troposphere the concentration of O_2 is on the order of 2×10^{19} molecules cm^{-3}, thus the lifetime of $CH_3OC(O)$ with respect to O_2 addition is expected to be on the order of microseconds. By contrast, reaction 25 has an estimated activation energy of 14.7 kcal mol^{-1} and an estimated Arrhenius factor of 10^{13} cm^3 $molecule^{-1}$ s^{-1}. Thus, the lifetime of $CH_3OC(O)$ with respect to unimolecular dissociation is expected to be on the order of milliseconds. These estimated lifetimes suggest that O_2 addition will be the dominant fate of the $CH_3OC(O)$ radical.

7. CH_2OCOH. CH_2OCOH can participate in the following reaction mechanisms:

$$CH_2OCOH \rightarrow CH_2O + HCO \quad (28)$$

$$CH_2OCOH \rightarrow CH_2 + HC(O)O \quad (29)$$

$$O_2 + CH_2OCOH \rightarrow O_2CH_2OCOH \quad (30)$$

Reaction 28 is a unimolecular CO cleavage reaction forming formaldehyde and the formyl radical. In the transition structure (Figure 2bb), the cleaving CO bond increases to 1.676 Å, while the opposing ether linkage bond decreases from 1.383 to 1.234 Å. The reaction illustrated in Figure 4b is endothermic by 20.5 kcal mol^{-1}, with a reaction barrier of 30.8 kcal mol^{-1}.

Reaction 29 is a CO cleavage reaction that forms CH_2 and HCO_2 radicals. The reaction is endothermic by 108.1 kcal mol^{-1} and is not expected to play a major role in the degradation mechanism. Even considering the potential formation of CO_2 through hydrogen ejection of HCO_2, a reaction enthalpy of 97.1 kcal mol^{-1} still exists.

In contrast to reactions 28 and 29, reaction 30 is a molecular oxygen addition reaction, which proceeds without barrier. The reaction enthalpy is predicted to be −37.6 kcal mol^{-1}. Again, the addition reaction is expected to dominate the possible reaction pathways.

$CH_3OC(O)O_2$ and O_2CH_2OCOH are each expected to follow one of the following reactions:

$$RO_2 + RO_2 \rightarrow 2RO + O_2 \quad (31)$$

$$RO_2 + NO \rightarrow RO + NO_2 \quad (32)$$

Each reaction leads to the formation of CH_3OCOO and OCH_2OCOH.

8. $CH_3OC(O)O$.

$$CH_3OC(O)O \rightarrow CH_3O + CO_2 \quad (33)$$

$$CH_3OC(O)O + O_2 \rightarrow HO_2 + CH_2O + CO_2 \quad (34)$$

The CO cleavage reaction in reaction 33 forms carbon dioxide and the methoxy radical. The reaction enthalpy was found to be −23.5 kcal mol^{-1} and the barrier height was found to be 13.0 kcal mol^{-1}. Reaction 34 is a hydrogen abstraction reaction initiated by O_2 (Figure 2aa). As the incoming O_2 atom removes the out-of-plane hydrogen atom, the CO_2 fragment is simulta-

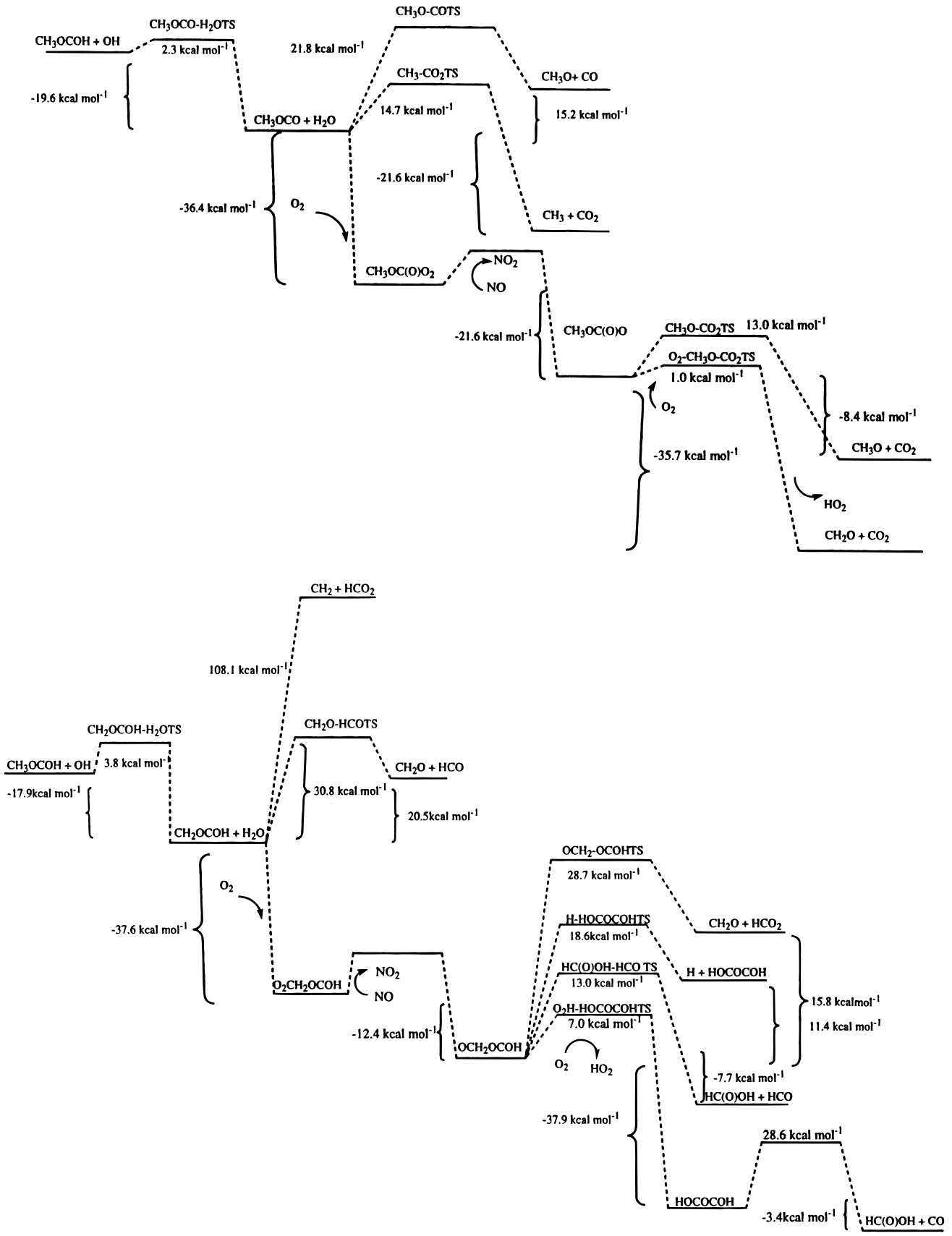

Figure 4. Energetics of the degradation pathways for methyl formate: (a) pathway following extraction of the carbonyl hydrogen; (b) pathway following extraction of the methyl hydrogen. Note: CH_2O-CH_3-SQTS refers to the four-center squarelike transition state represented in Figure 2p.

neously ejected. The dissociating CO bond has a length of over 2.790 Å. As shown in Table 10 and Figure 4a, the reaction is very favorable, with a reaction enthalpy of -50.8 kcal mol^{-1} and an activation energy of 1.0 kcal mol^{-1}. For this reaction the $\langle s^2 \rangle$ value is 0.79, which is above the expected value of 0.75.

TABLE 8: Reaction Pathways for Methyl Formate[a]

reaction	reaction enthalpy[b] G2	reaction enthalpy[b] G2(MP2)	reaction enthalpy[b] heat of formation	activation barrier G2	activation barrier G2(MP2)
$CH_3OCOH + OH \rightarrow CH_3OCO + H_2O$	−18.6	−19.2	−19.6	2.4	2.6
$CH_3OCOH + OH \rightarrow CH_2OCOH + H_2O$	−17.5	−18.1	−17.9	4.0	4.1
$CH_3OCOH + H_2O \rightarrow CH_3OH + HC(O)OH$	5.0	5.1	4.3	45.0	45.2

[a] All values in kcal mol^{-1}. [b] Reaction enthalpy computed at 298 K.

TABLE 9: Comparison of Decomposition Pathways for CH_3OCO and CH_2OCOH[a]

reaction	reaction enthalpy[b] G2	reaction enthalpy[b] G2(MP2)	reaction enthalpy[b] heat of formation	activation barrier G2	activation barrier G2(MP2)
$CH_3OCO \rightarrow CH_3 + CO_2$	−21.0	−21.0	−21.6	14.7	14.8
$CH_3OCO \rightarrow CH_3O + CO$	16.8	16.9	15.2	21.8	22.0
$CH_3OCO + O_2 \rightarrow CH_3OC(O)O_2$	−38.7	−39.2	−36.4	no barrier	no barrier
$CH_2OCOH \rightarrow CH_2O + HCO$	20.3	20.1	20.5	30.8	30.7
$CH_2OCOH \rightarrow CH_2 + HCO_2$	110.5	110.8	108.1	>110.5	>103.7
$CH_2OCOH + O_2 \rightarrow O_2CH_2OCOH$	−40.5	−41.1	−37.6	no barrier	no barrier

[a] All values in kcal mol^{-1}. [b] Reaction enthalpy computed at 298 K.

TABLE 10: Comparison of Decomposition Pathways for $CH_3OC(O)O$ and OCH_2OCOH[a]

reaction	reaction enthalpy[b] G2	reaction enthalpy[b] G2(MP2)	reaction enthalpy[b] heat of formation	activation barrier G2	activation barrier G2(MP2)
$CH_3OC(O)O \rightarrow CH_3O + CO_2$	−6.9	−7.2	−8.4	13.0	13.5
$CH_3OC(O)O + O_2 \rightarrow HO_2 + CH_2O + CO_2$	−38.7	−40.4	−35.7		1.0
$OCH_2OCOH \rightarrow CH_2O + HCO_2$	19.6	19.4	15.8	28.7	28.8
$OCH_2OCOH \rightarrow H + HOCOCOH$	9.9	9.3	11.4	18.6	18.4
$OCH_2OCOH + O_2 \rightarrow HO_2 + HOCOCOH$	−39.4	−40.6	−37.9		7.0
$OCH_2OCOH \rightarrow HC(O)OH + HCO$	−6.7	−7.3	−7.7		13.0

[a] All values in kcal mol^{-1}. [b] Reaction enthalpy computed at 298 K.

9. OCH_2OCOH. OCH_2OCOH can participate in the following pathways:

$$OCH_2OCOH \rightarrow H + HOCOCOH \quad (35)$$

$$OCH_2OCOH + O_2 \rightarrow HO_2 + HOCOCOH \quad (36)$$

$$OCH_2OCOH \rightarrow CH_2O + HC(O)OH \quad (37)$$

$$OCH_2OCOH \rightarrow HC(O)OH + HCO \quad (38)$$

Reaction 35 is a hydrogen ejection reaction forming formic acid anhydride. In the transition structure (Figure 2dd), the cleaving CH bond has a length of 1.535 Å. The reaction is endothermic by 11.4 kcal mol^{-1} and must overcome a reaction barrier of 18.6 kcal mol^{-1}.

Reaction 36 is another hydrogen abstraction reaction initiated by molecular oxygen. Figure 2ee shows the forming OH bond to be 1.340 Å, while the cleaving bond lengthens from 1.097 to 1.379 Å. The carbonyl CO bond decreases from 1.361 Å in OCH_2OCOH to 1.220 Å in the transition structure, and ultimately to 1.202 Å in formic acid anhydride. The energetics, as illustrated in Figure 4b, are favorable. The reaction enthalpy is −37.9 kcal mol^{-1}, with a reaction barrier of about 7.0 kcal mol^{-1}. As with the other hydrogen abstraction reactions initiated by molecular oxygen, the $\langle s^2 \rangle$ value is slightly higher (0.78) than the expected value for doublet systems.

Reaction 37, which is illustrated in Figure 2cc, results in the formation of CH_2O and HCO_2. In the transition structure, the dissociating CO bond lengthens to 1.928 Å, while the opposing single bond decreases to 1.335 Å. The reaction is found to be endothermic by 15.8 kcal mol^{-1} and has a reaction barrier of 28.7 kcal mol^{-1}.

Recent work by Tuazon et al.[50] suggests that alkoxy radicals of general structure RC(O)OCHOR isomerize through a five-membered ring transition structure to give RC(O)OH and RCO. The alkoxy radical $HC(O)OCH_2O$ would thus be expected to yield HC(O)OH and HCO, reaction 38. The transition structure is illustrated in Figure 2ff. The reaction is exothermic by −7.7 kcal mol^{-1} and must overcome a modest barrier of 13.0 kcal mol^{-1}. This reaction, along with the competing reaction 36, are both energetically favored reactions that result in the formation of formic acid.

10. HOCOCOH. The decomposition of formic acid anhydride has been found to produce *trans*-formic acid and carbon monoxide. The transition structure proposed by Lundell et al.[30] involves the simultaneous cleavage of one of the ether CO bonds and a hydrogen shift from the cleaving HCO fragment to the carbonyl oxygen of the HC(O)O fragment. Straight CO bond cleavage to produce HCO and HC(O)O is thought to be highly improbable.[30] The time constant for the formation of formic acid and carbon monoxide has been determined to be about 1 h at room temperature.[31] The transition structure for the formation of formic acid and CO is illustrated in Figure 2gg. This reaction is found to be exothermic by −3.4 kcal mol^{-1}.

11. HC(O)OH. There are several pathways by which formic acid can be removed. These could be by unimolecular decomposition or by reaction with OH radicals.

$$HC(O)OH \rightarrow CO + H_2O \quad (39)$$

$$HC(O)OH \rightarrow CO_2 + H_2 \quad (40)$$

$$HC(O)OH \rightarrow HC(O)O + H \quad (41)$$

$$HC(O)OH \rightarrow C(O)OH + H \quad (42)$$

$$HC(O)OH + OH \rightarrow H_2O + HC(O)O \rightarrow H + CO_2 \quad (43)$$

Processes 39 and 40 are unimolecular decomposition reactions referred to as the dehydration and decarboxylation reactions.

Reaction 40 is a decarboxylation reaction and has a slightly exothermic reaction enthalpy of -1.4 kcal mol^{-1}. Reaction 39 is a dehydration reaction, having an endothermic reaction enthalpy of 8.4 kcal mol^{-1}. Blake et al.[51] reported on the thermal decomposition of formic acid. The decarboxylation reaction was first order with a rate expression of k (s^{-1}) $= 10^{12.47}e^{-48.5/RT}$. For the dehydration reaction, two rates have been reported. For temperatures below 870 K, the rate was found to be second order, with a rate constant of k (cm^3 mol^{-1} s^{-1}) $= 10^{11.44}e^{-31.7/RT}$. For temperatures above 950 K, the rate was found to be of fractional order, with k (s^{-1}) $= 10^{15.39}e^{-60.5/RT}$.[51] Samsonov et al.[52] reported activation energies in the range 61.7−66.0 kcal mol^{-1} for the dehydration reaction. Evans et al.[53] suggested that the dissociation of formic acid could have free radical products, as illustrated by processes 41 and 42. However, shock tube studies in the 1280−2030 K by Hsu et al. concluded that such reactions were unimportant. Hsu et al.[54] reported threshold energies for the dehydration and decarboxylation reactions to be 62−65 and 65−68 kcal mol^{-1}, respectively. Saito et al.,[55] using shock tube methodology, determined a second-order reaction rate of the dehydration experiment to be k (cm^3 mol^{-1} s^{-1}) $= 10^{14.32}e^{-40.4/RT}$. Saito's ab initio calculations at the Hartree−Fock level using split valence basis sets showed the energy for the dehydration process to be 67.5 kcal mol^{-1}, while that for decarboxylation was 88.9 kcal mol^{-1}.[55] Francisco[56] investigated concerted molecular and bond fission unimolecular dissociation channels. Francisco[56] found the decarboxylation and dehydration channels to be energetically favored over rearrangement and radical reactions. Activation energies for the dehydration and decarboxylation reactions were consistent with the work of Hsu et al.[54] (63.0 and 65.2 kcal mol^{-1}, respectively).

Langford et al.[57] studied photodissociation dynamics of formic acid, including hydrogen bond cleaving reactions, producing radicals such as HCO_2 and CO_2H. Formic acid was vibronically excited at wavelengths between 216 and 240.86 nm. Following excitation, H atoms were detected using TOF mass spectrometry. Weak H atom signals were reported at wavelengths longer than 241 nm, due in part to weak parent absorption at these wavelengths.[57]

Both thermal and UV photodissociation pathways are unlikely to compete with hydroxyl radical initiated hydrogen abstraction reactions, reaction 43. Singleton et al.[58] showed that reactivity of HC(O)OH is essentially the same as that of DC(O)OH. DC(O)OD, however, was found to react much slower than HC(O)OH and DC(O)OH, showing that reaction proceeds via hydrogen abstraction of the acidic hydrogen. H atoms from the further dissociation of HCO_2 were also found by Wine et al.[59] and Jolly et al.[60]

IV. Conclusion

The major features of the atmospheric oxidation mechanism for dimethyl ether have been predicted theoretically. Atmospheric model studies of dimethyl ether show that the lifetime of dimethyl ether is expected to be 5.1 days. During that time, most of the dimethyl ether should degrade in the lower regions of the troposphere. Hydrogen abstraction from dimethyl ether, as initiated by the hydroxyl radical, is followed by O_2 addition to form methoxymethylperoxy radicals, $O_2CH_2OCH_3$, and ultimately, to methoxymethoxy radicals, OCH_2OCH_3. The fate of the methoxymethoxy radical is predicted to be dominated by conversion to methyl formate via a hydrogen abstraction mechanism initiated by molecular oxygen. The prediction of methyl formate as a byproduct of the oxidation of dimethyl ether is consistent with experimental observations. We have found that the oxidation of methyl formate can occur via two pathways. One pathway is initiated from the abstraction of the carbonyl hydrogen by the hydroxyl radical to form the CH_3OCO radical. The fate of CH_3OCO radicals is the conversion to CH_2O, CO_2, and HO_2 radicals. The second pathway results from the removal of a methyl hydrogen from methyl formate to form CH_2OCOH radicals, the fate of which is conversion to formic acid anhydride, HOCOCOH, through an oxygen addition and a hydrogen abstraction step also mediated by molecular oxygen. Formic acid anhydride ultimately rearranges to formic acid and carbon monoxide through a unimolecular rearrangement mechanism. Formic acid reacts with the hydroxyl radical to form CO_2, H_2O, and H atoms. The rate of this reaction is 4.0×10^{-13} molecule cm^{-3} s^{-1}. Using a simplistic expression for atmospheric lifetime ($\tau = 1/k$[OH], [OH] $\sim 10^6$ molecules cm^{-3}), formic acid is estimated to have an atmospheric lifetime of approximately one month. Alternatively, as suggested by Wine et al.,[59] formic acid may hydrogen bond with atmospheric water vapor, thus slowing its reactivity with the hydroxyl radical.[59] Under these conditions, heterogeneous processes such as wet or dry deposition of formic acid may compete. Industry is considering derivatives of dimethyl ether as possible fuel alternatives. It is expected that oxidation mechanisms of these derivatives can be modeled on the basis of properties such as the energetics found for the dimethyl ether system.

References and Notes

(1) Rouhi, A. M. *Chem. Eng. News* **1985**, *44*, 37.
(2) Askey, P. J.; Hinshelwood, C. N. *Proc. R. Soc. (London)* **1927**, *A115*, 215.
(3) Leifer, E.; Urey, H. C. *J. Am. Chem. Soc.* **1942**, *64*, 994.
(4) Benson, S. W. *J. Chem. Phys.* **1956**, *25*, 27.
(5) Benson, S. W.; Jain, D. V. S. *J. Chem. Phys.* **1959**, *31*, 1008.
(6) Pottie, R. F.; Harrison, A. G.; Lossing, F. P. *Can. J. Chem.* **1961**, *39*, 102.
(7) Nash, J. J.; Francisco, J. S. *J. Phys. Chem. A* **1998**, *102*, 36.
(8) Japar, S. M.; Wallington, T. J.; Richert, J. F. O.; Ball, J. C. *Int. J. Chem. Kinet.* **1990**, *22*, 1257.
(9) Jenkin, M. E.; Hayman, G. D.; Wallington, T. J.; Hurley, M. D.; Ball, J. C.; Nielsen, O. J.; Ellerman, T. *J. Phys. Chem.* **1993**, *97*, 11712.
(10) Wallington, T. J.; Hurley, M. D.; Ball, J. C.; Jenkin, M. E. *Chem. Phys. Lett.* **1993**, *211*, 41.
(11) Langer, S.; Ljungstrom, E.; Ellerman, T.; Nielsen, O. J.; Sehested, J. *Chem. Phys. Lett.* **1995**, *240*, 53.
(12) Sehested, J.; Mogelberg, T.; Wallington, T. J.; Kaiser, E. W.; Nielsen, O. J. *J. Phys. Chem.* **1996**, *100*, 17218.
(13) Sehested, J.; Sehested, K.; Platz, J.; Egsgaard, H.; Nielsen, O. J. *Int. J. Chem. Kinet.* **1997**, *29*, 627.
(14) Frisch, M. J.; Trucks, G. W.; Schlegel, H. B.; Gill, P. M. W.; Johnson, B. G.; Robb, M. A.; Cheeseman, J. R.; Keith, T.; Peterson, G. A.; Montgomery, J. A.; Raghavachari, K.; Al-Laham, M. A.; Zakrewski, V. G.; Ortiz, J. V.; Foresman, J. B.; Cioslowski, J.; Stefanov, B. B.; Nanayakkara, A.; Challacombe, M.; Peng, C. Y.; Ayala, P. Y.; Chen, W.; Wong, M. W.; Andres, J. L.; Replogle, E. S.; Gomperts, R.; Martin, R. L.; Fox, D. J.; Binkley, J. S.; DeFrees, D. J.; Baker, J.; Stewart, J. P.; Head-Gordon, M.; Gonzalez, C.; Pople, J. A. Gaussion94, revision D.2; Gaussian, Inc.: Pittsburgh, PA, 1995.
(15) Curtiss, L. A.; Raghavachari, K.; Trucks, G. W.; Pople, J. A. *J. Chem. Phys.* **1991**, *94*, 7221.
(16) Pople, J. A.; Head-Gordon, M.; Fox, D. J.; Raghavachari, K.; Curtiss, L. A. *J. Chem. Phys.* **1989**, *90*, 5622.
(17) Curtiss, L. A.; Raghavachari, K.; Pople, J. A. *J. Chem. Phys.* **1993**, *98*, 1293.
(18) Hehre, W. J.; Radom, L.; Schleyer, P. von, R.; Pople, J. A. *Ab Initio Molecular Orbital Theory;* Wiley: New York, 1986.
(19) Blukis, U.; Kasai, P. H.; Meyers, R. J. *J. Chem. Phys.* **1963**, *38*, 2753.
(20) Curl, R. F. *J. Chem. Phys.* **1959**, *30*, 1529.
(21) O'Gorman, J. M.; Shand, W.; Schomaker, V. *J. Am. Chem. Soc.* **1965**, *37*, 340.
(22) Jones, G. I. L.; Lister, D. G.; Owen, N. L.; Gerry, M. C. L.; Palmieri, P. *J. Mol. Spectrosc.* **1976**, *60*, 348.
(23) Wennerstrom, H.; Forsen, S.; Roos, B. *J. Phys. Chem.* **1972**, *76*, 2430.
(24) John, I. G.; Radom, L. *J. Mol. Spectrosc.* **1977**, *36*, 133.

(25) Nagy, P.; Kiss, A. I.; Lopata, A. *THEOCHEM* **1981**, *86*, 41.
(26) Subrahmanyam, S. V.; Piercy, J. E. *J. Acoust. Soc. Am.* **1965**, *37*, 340.
(27) Miyazawa, T. *Bull. Chem. Soc. Jpn.* **1961**, *34*, 691.
(28) Blom, C. E.; Günthard, Hs. H. *Chem. Phys. Lett.* **1981**, *84*, 267.
(29) Vaccani, S.; Roos, U.; Bauder, A.; Günthard, Hs. H. *Chem. Phys.* **1977**, *19*, 51.
(30) Lundell, J.; Rasanen, M.; Raaska, T.; Niemienen, J.; Murto, J. *J. Phys. Chem.* **1993**, *97*, 4577.
(31) Kühne, H.; Ha, T.-K.; Meyer, R.; Günthard, Hs. H. *J. Mol. Spectrosc.* **1979**, *77*, 251.
(32) Curran, H. J.; Pitz, W. J.; Westbrook, C. K.; Dagaut, P.; Buettner, J.-C.; Cathonnet, M. *Int. J. Chem. Kinet.* **1998**, *30*, 229.
(33) Good, D. A.; Francisco, J. S. *Chem. Phys. Lett.* **1997**, *266*, 512.
(34) Curtiss, L. A.; Raghavachari, K.; Redfern, P. C.; Pople, J. A. *J. Chem. Phys.* **1997**, *106*, 1063.
(35) Kondo, O.; Bensen, S. W. *J. Phys. Chem.* **1984**, *88*, 6675.
(36) Slagle, I. R.; Gutman, D. *J. Am. Chem. Soc.* **1985**, *107*, 5342.
(37) Knyazev, V.; Slagle, I. R. *J. Phys. Chem. A.* **1998**, *102*, 1770.
(38) Jungkamp, T. P. W.; Seinfeld, J. H. *Chem. Phys. Lett.* **1996**, *257*, 15.
(39) Lay, T. H.; Bozzelli, J. W. *J. Phys. Chem. A* **1997**, *101*, 9505.
(40) Maricq, M. M.; Szente, J. J.; Hybl, J. D. *J. Phys. Chem. A* **1997**, *101*, 5155.
(41) Louks, L. F.; Laidler, K. J. *Can. J. Chem.* **1967**, *45*, 2763.
(42) Good, D. A.; Francisco, J. S.; *J. Phys. Chem. A* **1998**, *102*, 7143.
(43) Wallington, T. J.; Liu, R.; Dagaut, P.; Kurylo, M. J. *Int. J. Chem. Kinet.* **1988**, *20*, 41.
(44) Wallington, T. J.; Ansino, J. M.; Skews, L. M.; Siegl, W. O.; Japar, S. M. *Int. J. Chem. Kinet.* **1989**, *21*, 993.
(45) Trully, F. P.; Droege, A. T. *Int. J. Chem. Kinet.* **1987**, *19*, 251.
(46) Perry, R. A.; Atkinson, R.; Pitts, J. N. *J. Chem. Phys.* **1977**, *67*, 611.
(47) Good, D. A.; Francisco, J. S.; Jain, A. K.; Wuebbles, D. J. *J. Geophys. Res.* **1998**, *103*, 28181.
(48) Le Calve' S.; Le Bras, G.; Mellouki, A. *J. Phys. Chem.* **1997**, *101*, 5489.
(49) DeMore, W. B.; Sander, S. P.; Golden, D. M.; Hampson, R. F.; Kurylo, M. J.; Howard, C. J.; Ravishankara, A. R.; Kolb., C. E.; Molina, M. J. *Chemical Kinetics and Photochemical Data for Use in Stratospheric Modeling Evaluation #12*; Jet Propulsion Laboratory: Pasadena, CA, January 1997.
(50) Tuazon, E. C.; Aschmann, S. M.; Atkinson, R.; Carter, W. P. L. *J. Phys. Chem. A* **1998**, *102*, 2316.
(51) Blake, P. G.; Davies, H. H.; Jackson, G. *J. Chem. Soc.* **1971**, 1923.
(52) Samsonov, Y. N.; Petrv, A. K.; Baklanov, A. V.; Vihzin, V. V. *React. Kinet. Catal. Lett.* **1976**, *5*, 197.
(53) Evans, D. K.; McAlpine, R. D.; McClusky, F. K. *Chem. Phys.* **1978**, *32*, 81.
(54) Hsu, D. S. Y.; Shaub, W. M.; Blackbum, M.; Lin, M. D. *The Nineteenth International Symposium on Combustion*; The Combustion Institute: Pittsburgh, PA, 1983; p 89.
(55) Saito, K.; Kakamoto, T.; Kuroda, H.; Torii, S.; Imamura, A. *J. Chem. Phys.* **1984**, *80*, 4989.
(56) Francisco, J. S. *J. Chem. Phys.* **1992**, *96*, 1167.
(57) Langford, S. R.; Batten, A. D.; Kono, M.; Ashford, M. N. R. *J. Chem. Soc., Faraday Trans.* **1997**, *93*, 3757.
(58) Singleton, D. L.; Paraskevpoulos, G.; Irwin, R. S.; Jolly, G. S.; McKenny, D. J. *J. Am. Chem. Soc.* **1988**, *110*, 7786.
(59) Wine, P. H.; Astalos, R. J.; Mauldin, R. L., III. *J. Phys. Chem.* **1985**, *89*, 2620.
(60) Jolly, G. S.; McKenny, D. J.; Singleton, D. L.; Paraskvpoulos, G.; Bossard, A. R. *J. Phys. Chem.* **1986**, *90*, 6557.